2013 21st Mediterranean Conference on Control & Automation (MED)
Platanias-Chania, Crete, Greece, June 25-28, 2013

A Received Signal Strength Indication-based Localization System

Pedro Lourenço, Pedro Batista, Paulo Oliveira, Carlos Silvestre, and Philip Chen

Abstract— **Localization using the received signal strength indication (RSSI) of wireless local area networks with a priori knowledge of the coordinates of the routers/access points is addressed in this paper. The proposed algorithm employs a path loss model that allows for the inclusion of the logarithmic measurements of the signal strength directly in the state of the nonlinear system that is designed. The nonlinear system is augmented in such a way that the resulting system structure may be regarded as linear time-varying for observability purposes, from which a Kalman filter follows naturally. Simulation results are included that illustrate the performance of the proposed solution.**

I. Introduction

The increasing use of mobile devices, such as smartphones, and the expansion of Wireless Local Area Network (WLAN) coverage have lead to an effort by the scientific community to develop localization algorithms using information provided by the Wi-Fi (WLAN using the IEEE 802.11 standard) signal. In indoor environments, where global positioning systems are not available, the cheap and lightweight nature of the Wi-Fi devices makes these kind of solutions more interesting. A good example of the use of wireless-based localization algorithms is the guidance of people inside sizeable buildings, such as museums or airports, using their own smartphones or other Wi-Fi capable devices.

Indoor environments pose a great challenge in this type of localization algorithms, as the connection between the router and the mobile antenna may not be line-of-sight, which leads to extra attenuation due to walls, floors, and people. In line-of-sight situations, there may occur multipath which impairs the localization, whichever the process employed may be. Several different approaches have been employed in the goal of developing Wi-Fi-based localization, namely the use of the angle-of-arrival, the time-of-arrival, and the signal power (see [1] for a survey of approaches). When using the signal power, different solutions have arisen, from the establishment of a signal finger print of the operating area, see [2] or, more recently, [3], to the use of path loss models, [4] and [5]. The solution proposed in this paper fits in the last category.

This paper addresses the design, analysis and validation through simulation of an algorithm for localization using the received signal strength from known routers. A propagation model is employed to convert the received signal strength indication (RSSI) into ranges. Given that the information provided by the Wi-Fi devices regarding the signal power (RSSI) is expressed in dBm, the logarithm of the ranges is directly fed to the filter without further computation, thus avoiding the introduction of multiplicative noise. This is suggested by the Gaussian behaviour of the logarithmic measurements confirmed by the experimental survey in [6]. The algorithm proposed in this paper builds on the work exposed in [7] in the sense that a nonlinear system is derived and augmented in such a way that the resulting system may be considered as linear time-varying, without any linearization or approximation whatsoever, as it resorts to exact linear and angular motion kinematics. The sensor suite used encompasses a Wi-Fi device for the power measurements and an IMU for obtaining the angular rates. The main contribution of this work is the use of the logarithm of the ranges both as a state and output of the system that defines the proposed filter.

The paper is organized as follows. Section II presents a short description of the problem, while introducing the motivation for the use of the logarithm of the ranges as a measurement. The system dynamics are derived in Section III and the observability analysis is performed in Section IV. The filter design is addressed in Section V and simulation results are presented in Section VI. Finally, some conclusions and future work directions are detailed in Section VII.

A. Notation

The superscript ^{I} indicates a vector or matrix expressed in the inertial frame $\{I\}$. For the sake of clarity, when no superscript is present, the vector is expressed in the body-fixed frame $\{B\}$. $\mathbf{I}_n$ is the identity matrix of dimension n, and $\mathbf{0}_{n\times m}$ is a n by m matrix filled with zeros. When the dimensions are omitted the matrices are assumed of appropriate dimensions. $\mathbf{S}[\mathbf{a}]$ is a special skew-symmetric matrix, henceforth called the cross-product matrix, as $\mathbf{S}[\mathbf{a}]\mathbf{b} = \mathbf{a}\times\mathbf{b}$ with $\mathbf{a},\mathbf{b}\in\mathbb{R}^3$. The operators $\log$ and $\ln$ represent the base 10 logarithm and the natural one, respectively.

II. Description of the problem

This section addresses the problem of designing a localization algorithm for an agent operating in an environment where several Wi-Fi routers or access points are present. The algorithm uses the received signal power, or, more accurately, the received signal strength indication (RSSI) levels, as ranges to the previously known routers. Hence, the filter must use a propagation model for the received signals to relate the power of the received signal to the actual distance from the receiver to the router. The free space propagation

This work was partially supported by the FCT [PEst-OE/EEI/LA0009/2011] and by the EU Project TRIDENT (Contract No. 248497). The work of Pedro Lourenço was supported by the PhD Student Grant SFRH/BD/89337/2012 from the Portuguese FCT POCTI programme.

Pedro Lourenço, Pedro Batista, Paulo Oliveira, and Carlos Silvestre are with the Institute for Systems and Robotics, Instituto Superior Técnico, Universidade Técnica de Lisboa, Av. Rovisco Pais, 1049-001 Lisboa, Portugal. Carlos Silvestre and Philip Chen are with the Faculty of Science and Technology of the University of Macau.

{plourenco,pbatista,pjcro,cjs}@isr.ist.utl.pt and philipchen@umac.mo

model for electromagnetic waves is given by

$$P_{RX} = \frac{P_{TX} G_{TX} G_{RX} \lambda^2}{(4\pi)^2 r^2},$$

where the RX and TX subscripts represent the receiver and router, P is the power in Watt, G is the antenna gain, λ is the wavelength, and r is the distance between the router and the receiver. Although this is a theoretical situation, it hints at the logarithmic relation between the received power in dB and the distance that is confirmed by the empirical models arose to better express the path loss, ie., the ratio $\frac{P_{TX}}{P_{RX}}$. One example is the logarithmic path loss model [6]

$$\frac{P_{TX}}{P_{RX}}(dB) \propto r^n,$$

where n is the path loss exponent (dependent of the environment). A similar version of this model is the Hata-Okumura model (see [1] and [8])

$$\log r_m = \frac{1}{10n}\left(P_{TX} - P_{RX} + G_{TX} + G_{RX} - X_{\sigma_{RX}} + 20\log\lambda - 20\log(4\pi)\right), \quad (1)$$

where all the powers are expressed in dBm and the gains in dBi. The random variable $X_{\sigma_{RX}}$ is a normal distributed zero mean quantity with a standard deviation of σ_{RX} that represents the noise in the measurement, and r_m is the noisy range.

Both models were designed to account for outdoor propagation, but [1] proposes a variation of this model which accommodates the influence of partitions, doors and walls, thus producing a model for indoor propagation. The referred influence is hidden in the parameter n and in σ_{RX}. If the average received power is known at a predefined distance r_0, then the model (1) becomes

$$\log\frac{r_m}{r_0} = -\frac{1}{10n}\left(P_{RX} - P_{RX_0} + X_{\sigma_{RX}} - X_{\sigma_{RX_0}}\right),$$

which may be rearranged to obtain the distance through

$$r_m = r_0\ 10^{-\frac{1}{10n}\left(P_{RX} - P_{RX_0}\right)}\ 10^{-\frac{1}{10n}\left(X_{\sigma_{RX}} - X_{\sigma_{RX_0}}\right)}. \quad (2)$$

The work in [1] includes a Wi-Fi survey that leads to the conclusion that the RSSI readings are normal distributed. Hence, computing the measured ranges r_m from the measured logarithmic power will introduce noise that depends on the distance, as the expansion of (2) shows

$$r_m = r\ 10^u = r + r\sum_{n=1}^{\infty}\frac{(u\ln 10)^n}{n!},$$

where u is the Gaussian noise that disturbs the logarithmic measurements. Knowing this, it makes sense to use the logarithmic power measurements directly in a filtered trilateration technique, instead of computing r_m.

A. Model Validation

To evaluate the validity of this hypothesis, a sample of 3600 RSSI readings was collected with both antennas static. Given that the RSSI readings are integers, this sample was compared with a normal-distributed random sequence with the same variance and mean rounded to the nearest integer. The results of this survey are shown in Fig. 1, which depicts the normality plots of both the acquired sample (in Fig. 1(a)) and the random sample (in Fig. 1(b)). It can be seen that in both samples there is a deviation from the normal red line when the values move away from the mean, although the deviation is more noticeable in higher power values in the acquired sample.

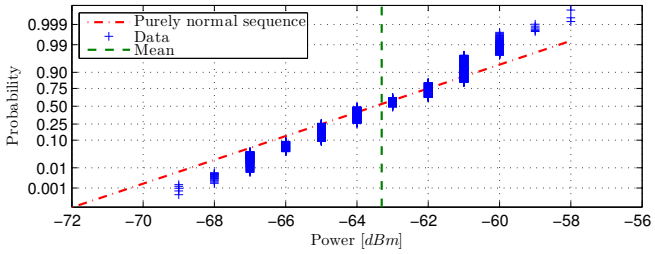

(a) RSSI readings.

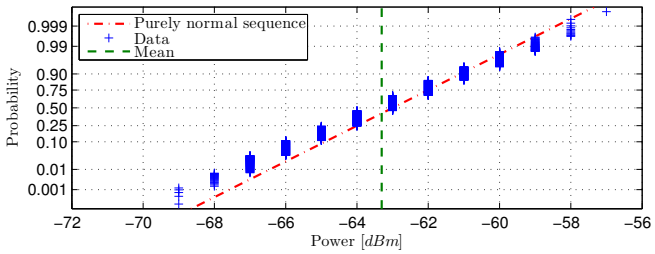

(b) Rounded random sample.

Fig. 1. Normality plots.

Aside from the validation of the Gaussian hypothesis, an experiment was conducted with the purpose of validating the logarithmic model. The experiment consisted in moving a Wi-Fi antenna in a room equipped with a 5GHz router and ground truth, and then comparing the distance between the router and the antenna with the ranges calculated through the calibrated model (2). The result depicted in Fig. 2 shows that the computed ranges follow the tendency of the ground truth, although there are significant mismatches, possibly due to reflections.

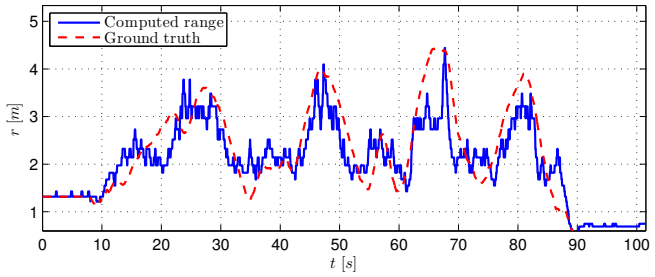

Fig. 2. Range computed using model (2) against ground truth data.

B. Problem Statement

The problem addressed in this paper is the design of a localization filter using the coordinates of the router positions and the received signal strength in logarithmic units.

III. System Dynamics

The model presented in the previous section suggests that the observations to be used in this localization filter are

indeed the logarithm of the distance and not the distance itself. Thus, these will be the output of the system in design.

Let ${}^I\mathbf{p}(t) \in \mathbb{R}^3$ be the position of the agent in a local inertial frame denoted by $\{I\}$, and $\mathbf{s}_i \in \mathbb{R}^3$, $i \in \{1, \dots, N\}$, be the position in the same frame of the i-th hot-spot, henceforth denominated landmark. The linear motion of the agent is then given by

$$\begin{cases} {}^I\dot{\mathbf{p}}(t) = {}^I\mathbf{v}(t) \\ {}^I\dot{\mathbf{v}}(t) = {}^I\mathbf{a}(t) \end{cases},$$

where ${}^I\mathbf{v}(t) \in \mathbb{R}^3$ is the linear velocity and ${}^I\mathbf{a}(t) \in \mathbb{R}^3$ is the linear acceleration of the agent. The motion is considered to be slowly time-varying, and therefore, in a deterministic setting, ${}^I\dot{\mathbf{a}}(t) = 0$.

Consider that the landmarks are static and that the landmark positions are known. Then, each output of the system is given by

$$\log r_i(t) = \log \|\mathbf{s}_i - {}^I\mathbf{p}(t)\|$$

for all $i \in \{1, \dots, N\}$. The resulting system is given by

$$\begin{cases} {}^I\dot{\mathbf{p}}(t) = {}^I\mathbf{v}(t) \\ {}^I\dot{\mathbf{v}}(t) = {}^I\mathbf{a}(t) \\ {}^I\dot{\mathbf{a}}(t) = \mathbf{0} \\ \log r_1(t) = \log \|\mathbf{s}_1 - {}^I\mathbf{p}(t)\| \\ \vdots \\ \log r_N(t) = \log \|\mathbf{s}_N - {}^I\mathbf{p}(t)\| \end{cases} \tag{3}$$

where all quantities are expressed in the inertial frame.

Due to the nature of the outputs of the system, it is clear that it is nonlinear. In order for a linear, or, in fact, linear time-varying, Kalman filter to be designed, a new system that mimics the dynamics of (3) must be derived, following a similar approach to that successfully proposed in [7].

A. State augmentation

In order to derive a system that can be seen as linear and that mimics the dynamics of the nonlinear system (3), new quantities must be added to the original system, in the form of the following $N + 4$ additional scalar states:

$$\begin{cases} x_4(t) = \log r_1(t) \\ \vdots \\ x_{N+3}(t) = \log r_N(t) \\ x_{N+4}(t) = \mathbf{x}_1(t)^T \mathbf{x}_2(t) \\ x_{N+5}(t) = \mathbf{x}_1(t)^T \mathbf{x}_3(t) + \|\mathbf{x}_2(t)\|^2 \\ x_{N+6}(t) = \mathbf{x}_3(t)^T \mathbf{x}_2(t) \\ x_{N+7}(t) = \|\mathbf{x}_3(t)\|^2 \end{cases}, \tag{4}$$

where $\mathbf{x}_1(t) := {}^I\mathbf{p}(t)$, $\mathbf{x}_2(t) := {}^I\mathbf{v}(t)$ and $\mathbf{x}_3(t) := {}^I\mathbf{a}(t)$, leading to the new system state $\mathbf{x}(t) = \begin{bmatrix} \mathbf{x}_1^T(t) & \cdots & \mathbf{x}_3^T(t) & x_4(t) & \cdots & x_{N+7}(t) \end{bmatrix}^T$.

The inclusion of the logarithm of the ranges in the system state makes the relation between the system output and state linear, and the four remaining quantities will enable the system dynamics to be considered as linear time-varying.

B. Output augmentation

For the completion of the proposed framework, a further step is needed. Consider the expansion of the square of the range to a landmark, given by

$$r_i^2(t) = \|\mathbf{s}_i\|^2 + \|{}^I\mathbf{p}(t)\|^2 - 2\mathbf{s}_i^T {}^I\mathbf{p}(t).$$

The subtraction of the square of the ranges to two different landmarks i and j leads to the following expression

$$2\frac{(\mathbf{s}_i - \mathbf{s}_j)^T \mathbf{x}_1(t)}{r_i(t) + r_j(t)} = \frac{\|\mathbf{s}_i\|^2 - \|\mathbf{s}_j\|^2}{r_i(t) + r_j(t)} - (r_i(t) - r_j(t)),$$

$i, j \in 1, \dots, N, i \neq j$, where the agent position was substituted by the corresponding state vector. Note that the right-hand side is known, as it is a function of the system output, with the ranges being calculated through the propagation model (2). Furthermore, the term that multiplies $\mathbf{x}_1(t)$ is also known. The various combinations of this expression are added as system outputs, thus allowing to write the final augmented system output as $\mathbf{y}(t) = \begin{bmatrix} y_1(t) & \cdots & y_{N+C_2^N}(t) \end{bmatrix}$, with

$$\begin{cases} y_i(t) = x_{3+i}(t) \\ y_{N+j}(t) = 2\frac{(\mathbf{s}_l - \mathbf{s}_l)^T \mathbf{x}_1(t)}{r_k(t) + r_l(t)}, \end{cases}$$

where $i, k, l = 1, \dots, N$, $j = 1, \dots, C_2^N$ and $l > j$.

With the state and output augmentation completed, it is now possible to write the augmented system dynamics, resulting in

$$\begin{cases} \dot{\mathbf{x}}(t) = \mathbf{A}(t)\mathbf{x}(t) \\ \mathbf{y}(t) = \mathbf{C}(t)\mathbf{x}(t) \end{cases}, \tag{5}$$

where

$$\mathbf{A}(t) = \begin{bmatrix} \mathbf{0} & \mathbf{I} & \mathbf{0} & \mathbf{0} & \cdots & \mathbf{0} & \mathbf{0} & \mathbf{0} & \mathbf{0} & \mathbf{0} \\ \mathbf{0} & \mathbf{0} & \mathbf{I} & \mathbf{0} & \cdots & \mathbf{0} & \mathbf{0} & \mathbf{0} & \mathbf{0} & \mathbf{0} \\ \mathbf{0} & \mathbf{0} & \mathbf{0} & \mathbf{0} & \cdots & \mathbf{0} & \mathbf{0} & \mathbf{0} & \mathbf{0} & \mathbf{0} \\ \mathbf{0} & -\frac{\mathbf{s}_1^T}{r_1^2(t)} & \mathbf{0} & \mathbf{0} & \cdots & \mathbf{0} & \frac{1}{r_1^2(t)} & 0 & 0 & 0 \\ \vdots & \vdots & \vdots & \vdots & \vdots & \vdots & \vdots & \vdots & \vdots & \vdots \\ \mathbf{0} & -\frac{\mathbf{s}_N^T}{r_N^2(t)} & \mathbf{0} & \mathbf{0} & \cdots & \mathbf{0} & \frac{1}{r_N^2(t)} & 0 & 0 & 0 \\ 0 & 0 & 0 & 0 & \cdots & 0 & 0 & 1 & 0 & 0 \\ 0 & 0 & 0 & 0 & \cdots & 0 & 0 & 0 & 3 & 0 \\ 0 & 0 & 0 & 0 & \cdots & 0 & 0 & 0 & 0 & 1 \\ 0 & 0 & 0 & 0 & \cdots & 0 & 0 & 0 & 0 & 0 \end{bmatrix}, \tag{6}$$

and

$$\mathbf{C}(t) = \begin{bmatrix} \mathbf{0}_{N\times 3} & \mathbf{0}_{N\times 3} & \mathbf{0}_{N\times 3} & \mathbf{I}_N & \mathbf{0}_{N\times 4} \\ \mathbf{C}_{aug}(t) & \mathbf{0}_{C_2^N\times 3} & \mathbf{0}_{C_2^N\times 3} & \mathbf{0}_{C_2^N\times N} & \mathbf{0}_{C_2^N\times 4} \end{bmatrix}, \tag{7}$$

with

$$\mathbf{C}_{aug}(t) = 2\begin{bmatrix} \mathbf{c}_{a_{12}}^T(t) & \mathbf{c}_{a_{13}}^T(t) & \cdots & \mathbf{c}_{a_{(N-2)N}}^T(t) & \mathbf{c}_{a_{(N-1)N}}^T(t) \end{bmatrix}^T,$$

where $\mathbf{c}_{a_{ij}}(t) = (\mathbf{s}_i - \mathbf{s}_j)^T (r_i(t) + r_j(t))^{-1}$.

As referred, although system (5) is nonlinear, it may be regarded as a linear time varying system for observability purposes, provided that the system output is known.

Note that, as long as the agent is not at the same position of a landmark, i.e $r_i(t) > 0 \quad \forall i \in \{1, \dots, N\}$, (6) is always

well-defined. Another important fact to take into account when analysing this system is that its dynamics do not impose any of the algebraic restrictions stated by (4).

IV. Observability Analysis

The work exposed in this section aims at analysing the observability of the dynamical system derived in the previous section. It is important to notice that, although system (5) is inherently nonlinear due to the presence of the ranges in the dynamics and output matrices, the relation between the ranges and part of the output of the system makes it possible to consider these matrices as functions of the system output, which is known, thus allowing to consider the whole system as linear time-varying. Linear systems theory may thus be employed to establish sufficient conditions for the observability of the LTV system with a physical interpretation. These results are then extended to the original nonlinear system, allowing the design of a state observer for the original nonlinear system.

Classic linear system results relate the invertibility of the observability Gramian associated with a linear time-varying system with the observability of the same system. [9, Lemma 1] states that, if the observability Gramian associated with the pair $(\mathbf{A}(t), \mathbf{C}(t))$, possibly dependent on the system output and input, is invertible, then the system is observable. This result will be used in the following theorem that addresses the observability of system (5).

Theorem 1: Let $\mathcal{T} := [t_0, t_f]$ and consider system (5). Given the system output $\{\mathbf{y}(t), t \in \mathcal{T}\}$, the system is observable in the sense that the initial condition $\mathbf{x}(t_0)$ is uniquely defined, provided that

i. there exist at least 4 non-coplanar landmarks, and
ii. $\underset{R_M, R_m > 0}{\exists} \quad \underset{t \geq t_0}{\forall} \quad R_m \leq r_i(t) \leq R_M,\ i \in 1, \ldots, N.$

Proof: The proof consists in showing that the observability Gramian is invertible in the conditions expressed.

The computation of the observability Gramian requires the knowledge of the transition matrix $\boldsymbol{\phi}(t, t_0)$ for the system (5), which may, in this case, be simply computed by solving

$$\mathbf{x}(t) = \boldsymbol{\phi}(t, t_0)\mathbf{x}(t_0) = \mathbf{x}(t_0) + \int_{t_0}^{t} \mathbf{A}(y(\sigma), \sigma)\mathbf{x}(\sigma) d\sigma.$$

Recall that if the observability Gramian $\boldsymbol{\mathcal{W}}(t_0, t_f)$ is invertible, the system (5) is observable, in the sense that given the system input and output, the initial condition $\mathbf{x}(t_0)$ is uniquely defined. The proof follows by contradiction, i.e., by supposing that $\boldsymbol{\mathcal{W}}(t_0, t_f)$ is singular. Then, there exists a unit vector $\mathbf{c} = \begin{bmatrix} \mathbf{c}_1^T & \mathbf{c}_2^T & \mathbf{c}_3^T & \mathbf{c}_4^T & c_5 & c_6 & c_7 & c_8 \end{bmatrix}^T$, with $\mathbf{c}_1, \mathbf{c}_2, \mathbf{c}_3 \in \mathbb{R}^{3\times 1}$, $\mathbf{c}_4 \in \mathbb{R}^{N\times 1}$ and the remaining c_is being scalars, such that

$$\mathbf{c}^T \boldsymbol{\mathcal{W}}(t_0, t_f)\mathbf{c} = \int_{t_0}^{t_f} \|\mathbf{f}(\tau, t_0)\|^2 d\tau = 0. \tag{8}$$

The proof follows by showing that there is no such unit vector $\mathbf{c}$, if the conditions of the theorem apply, that satisfies (8). In order for this to be true, both $\mathbf{f}(\tau, t_0)$ and $\frac{d\mathbf{f}(\tau, t_0)}{d\tau}$ must be zero $\forall \tau \in \mathcal{T}$. Using the transition matrix and (7) in (8) yields

$$\mathbf{f}(\tau, t_0) = \begin{bmatrix} f_1(\tau, t_0) \\ \vdots \\ f_N(\tau, t_0) \\ f_{12}(\tau, t_0) \\ f_{13}(\tau, t_0) \\ \vdots \\ f_{(N-2)N}(\tau, t_0) \\ f_{(N-1)N}(\tau, t_0) \end{bmatrix}, \tag{9}$$

where

$$f_i(\tau, t_0) = -\mathbf{s}_i^T r_i^{[0]}(\tau)\mathbf{c}_2 - \mathbf{s}_i^T r_i^{[1]}(\tau)\mathbf{c}_3 + c_{4_i} + r_i^{[0]}(\tau)c_5 + r_i^{[1]}(\tau)c_6 + \frac{3}{2} r_i^{[2]}(\tau)c_7 + \frac{1}{2} r_i^{[3]}(\tau)c_8,$$

and

$$f_{jk}(\tau, t_0) = \frac{(\mathbf{s}_j - \mathbf{s}_k)^T}{r_j(\tau) + r_k(\tau)} \left(2\mathbf{c}_1 + 2(\tau - t_0)\mathbf{c}_2 + (\tau - t_0)^2 \mathbf{c}_3\right),$$

with $r_i^{[n]}(\tau) = \int_{t_0}^{\tau} r_i^{-2}(\sigma)\,(\sigma - t_0)^n\, d\sigma$.

Setting $\tau = t_0$ in (9) while computing $\mathbf{f}(t_0, t_0) = \mathbf{0}$ yields

$$\mathbf{f}(\tau, t_0) = \begin{bmatrix} \mathbf{c}_4 \\ \mathbf{C}_{aug}(t_0)\mathbf{c}_1 \end{bmatrix} = 0,$$

which in turn yields $\mathbf{c}_4 = 0$ and, if condition (ii) applies, $\mathbf{c}_1 = 0$. Note that condition (ii) is equivalent to $\operatorname{rank}(\mathbf{C}_{aug}(t)) = 3$.

Taking the first time derivative of $f_i(\tau, t_0) = 0$ yields

$$-r_i^{-2}(\tau)\mathbf{s}_i^T\mathbf{c}_2 - (\tau - t_0)r_i^{-2}(\tau)\mathbf{s}_i^T\mathbf{c}_3 + r_i^{-2}(\tau)c_5 + (\tau - t_0)r_i^{-2}(\tau)c_6 + \frac{3}{2}(\tau - t_0)^2 r_i^{-2}(\tau)c_7 + (\tau - t_0)^3 \frac{1}{2} r_i^{-2}(\tau)c_8 = 0.$$

If condition (i) applies, this expression can be rewritten as

$$-\mathbf{s}_i^T\mathbf{c}_2 - (\tau - t_0)\mathbf{s}_i^T\mathbf{c}_3 + c_5 + (\tau - t_0)c_6 + \frac{3}{2}(\tau - t_0)^2 c_7 + (\tau - t_0)^3 \frac{1}{2} c_8 = 0, \tag{10}$$

and, if evaluated at $\tau = t_0$, expression (10) becomes

$$\mathbf{s}_i^T\mathbf{c}_2 = c_5. \tag{11}$$

The evaluation at $\tau = t_0$ of the derivative of (10) yields

$$\mathbf{s}_i^T\mathbf{c}_3 = c_6. \tag{12}$$

Again, assuming that (ii) applies, (11) and (12) yield $\mathbf{c}_2 = \mathbf{c}_3 = \mathbf{0}$ and $c_5 = c_6 = 0$. Using this result in (10) and noting that $(\tau - t_0)^2$ and $(\tau - t_0)^3$ are all linearly independent finally yields $c_7 = c_8 = 0$. This, in turn, means that $\mathbf{c} = 0$, hence, $\mathbf{c}$ is not a unit vector, $\boldsymbol{\mathcal{W}}(t_0, t_f)$ is invertible, and system (5) is observable. ■

This result shows that, given the conditions established, the initial state of the augmented system is uniquely defined. Nevertheless, at first sight, given that there is nothing imposing the algebraic restrictions that lead to the augmented states in the first place, the observability of the augmented system does not imply that the original nonlinear system is observable. The following theorem addresses this issue.

Theorem 2: Consider that the conditions of Theorem 1 hold. Then, the initial state of the nonlinear system (3) is uniquely determined, and is the same of the nonlinear system (5), meaning that system (3) is observable. Furthermore, the algebraic restrictions (4) become naturally imposed by the system dynamics.

Proof: The proof is made by comparison of the output of the two systems in analysis to show the correspondence of their initial conditions. The explicit evolution of the squared ranges with the initial states is computed and used to obtain the correspondence of the augmented states. The proof is omitted due to lack of space, although the reader is referred to [10] for a similar proof. ■

V. Filter Design and Implementation

This section addresses the design of a filter for the nonlinear system proposed in this paper, by means of the augmented system previously designed. Although a filter could be designed directly for this system, the acquisition of the logarithmic ranges may be a low-bandwidth process, and therefore it is of interest to include information from higher bandwidth sensors so that better estimates may be provided at higher rates. For that purpose, the augmented system (5) is transformed using a Lyapunov transformation (see [11] for details).

Let $\mathbf{R}(t) \in \mathrm{SO}(3)$ be the rotation matrix that, along with the agent position ${}^{I}\mathbf{p}(t)$, transforms a vector from the body-fixed frame $\{B\}$ to the local inertial frame $\{I\}$. This rotation matrix respects the relation $\dot{\mathbf{R}}(t) = \mathbf{R}(t)\mathbf{S}\left[\boldsymbol{\omega}(t)\right]$ where $\boldsymbol{\omega}(t) \in \mathbb{R}^3$ is the angular velocity expressed in the body-fixed frame.

Consider now the Lyapunov transformation

$$\mathbf{T}(t) = \mathrm{diag}\left(\mathbf{I}_3, \mathbf{R}^T(t), \mathbf{R}^T(t), \mathbf{I}_N, 1, 1, 1, 1\right), \qquad (13)$$

and the new system state $\boldsymbol{\chi}(t) = \mathbf{T}(t)\mathbf{x}(t)$. Note that, in this new state, the linear velocity and acceleration are rotated to the body-fixed frame. The resulting system dynamics are given by

$$\begin{cases} \dot{\boldsymbol{\chi}}(t) = \boldsymbol{\mathcal{A}}(t)\boldsymbol{\chi}(t) \\ \mathbf{y}(t) = \mathbf{C}(t)\boldsymbol{\chi}(t) \end{cases}, \qquad (14)$$

where the dynamics matrix, depending on the angular velocity and the rotation matrix, is

$$\boldsymbol{\mathcal{A}}(t, \boldsymbol{\omega}(t), \mathbf{R}(t), \mathbf{y}(t)) = \dot{\mathbf{T}}(t)\mathbf{T}^T(t) + \mathbf{T}(t)\mathbf{A}(t)\mathbf{T}^T(t).$$

This new system dynamics is guided by the angular velocity measurements provided by a triad of orthogonally mounted rate-gyros, which usually have a high sampling rate as required. It is important to notice that, given that system (14) is related to system (5) through a Lyapunov transformation, the observability results of the previous section also apply to the new system.

Due to the discrete nature of the sensors employed, a discrete time Kalman filter was designed. Hence, the system to be estimated has to be redefined. Denoting the fundamental sampling period as T_s, the discrete time steps can be expressed as $t_k = kT_s + t_0$, $k \in \mathbb{N}_0$ and t_0 denotes the initial time. Thus, the discretized system is characterized by the state $\mathbf{x}_k := \boldsymbol{\chi}(t_k)$, the dynamics matrix $\mathbf{A}_k := \boldsymbol{\mathcal{A}}(t_k)$ and the output matrix $\mathbf{C}_k := \mathbf{C}(t_k)$. Finally, the Euler discretization of the system dynamics (14) including system disturbance and measurement noise yields

$$\begin{cases} \mathbf{x}_{k+1} = \mathbf{F}_k\mathbf{x}_k + \boldsymbol{\xi}_k \\ \mathbf{y}_{k+1} = \mathbf{H}_{k+1}\mathbf{x}_{k+1} + \boldsymbol{\theta}_{k+1} \end{cases},$$

where $\mathbf{F}_k := \mathbf{I}_{n_x} + T_s\mathbf{A}_k$ and $\mathbf{H}_{k+1} := \mathbf{C}_{k+1}$. The disturbance vector $\boldsymbol{\xi}_k$ and the measurement noise vector $\boldsymbol{\theta}_k$ are both zero-mean discrete white Gaussian noise, with $\langle \boldsymbol{\xi}_k \boldsymbol{\xi}_k^T \rangle = \boldsymbol{\Xi}_k$ and $\langle \boldsymbol{\theta}_k \boldsymbol{\theta}_k^T \rangle = \boldsymbol{\Theta}_k$, respectively. This system is filtered through a standard LTV Kalman filter.

Note that the system fully designed in the inertial frame could be implemented directly, without resorting to the Lyapunov transformation (13). In fact, the inertial frame solution is simpler to implement, as its only inputs are the RSSI measurements. Therefore, it is possible to use it with less sensors, and cheaper equipment. The sensor-based filter demands more inputs, needing to be fed by an attitude estimator and rate-gyros for the angular rate measurements, aside from the compulsory RSSI measurements.

VI. Simulation results

This section presents the results of a simulation assuming that the RSSI readings are logarithmic with a standard deviation of $1.5\ \mathrm{dBm}$. The attitude is noisy, with the additive Gaussian noise having a standard deviation of $0.03°$ for the roll and pitch and $0.3°$ for yaw. The angular speeds are corrupted by additive, uncorrelated, zero-mean white Gaussian noise with standard deviations of $0.05°/s$. The simulated environment consists of 4 non-coplanar landmarks with the following coordinates

$$\mathbf{s}_1 = \begin{bmatrix} 0 & 8 & -1 \end{bmatrix}^T m, \qquad \mathbf{s}_2 = \begin{bmatrix} 8 & 0 & 3 \end{bmatrix}^T m,$$
$$\mathbf{s}_3 = \begin{bmatrix} 16 & 8 & -1 \end{bmatrix}^T m, \qquad \mathbf{s}_4 = \begin{bmatrix} 8 & 16 & 3 \end{bmatrix}^T m,$$

in a $16\mathrm{m}\times16\mathrm{m}\times4\mathrm{m}$ map, including a closed $2\mathrm{m}$ wide corridor in the outer borders of the map. The trajectory is simply a loop through the corridors at half-height, with the agent starting on the floor. The simulated map and trajectory can be found in Fig. 3 along with the estimated path.

The tunable parameters of the Kalman filter are the model disturbance noise covariance and the measurement noise covariance given by, respectively, $\boldsymbol{\Xi} = \mathrm{diag}\left(10^{-10}\mathbf{I}_3, 10^{-10}\mathbf{I}_3, 10^{-6}\mathbf{I}_3, 10^{-2}\mathbf{I}_4, \boldsymbol{\Xi}_{aug}\right)$ and $\boldsymbol{\Theta} = \mathrm{diag}\left(10^{-2}\mathbf{I}_4, 2.25\mathbf{I}_6\right)$, where $\boldsymbol{\Xi} = \mathrm{diag}(9 \times 10^{-20}, 9 \times 10^{-16}, 9 \times 10^{-16}, 9 \times 10^{-12})$.

Firstly, the localization performance can be evaluated through Fig. 3 and Fig. 5. The former depicts the estimated path (in green) against the true path (in red). The latter presents the estimation error of the position estimate (Fig. 5(a)), the velocity estimate (Fig. 5(b)), the acceleration (Fig. 5(c)). It is important to note that estimation error of the vertical coordinates is greater than that of the horizontal ones, due to smaller vertical distance when compared to the horizontal. In fact, being this a long baseline-like filter, the distances between landmarks should be greater or comparable to the distance between the agent and the landmarks.

The evolution of the uncertainty of the filter estimates can be found in Fig. 4, depicting the position, velocity and acceleration standard deviations. Note the convergence of the uncertainty in the first 50 seconds when the agent was stopped, confirming the theoretical results of Section IV.

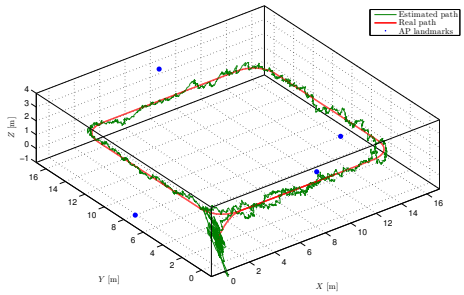

Fig. 3. Real and estimated path.

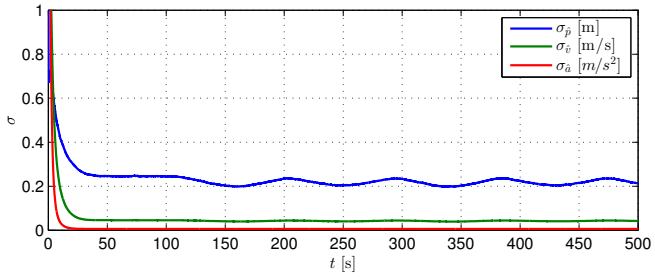

Fig. 4. Standard deviation of the main state variables.

This simulation enabled the confirmation of the theoretical results obtained, as well as the demonstration of the coherence of the uncertainty of the estimation with the actual estimation error.

VII. Conclusions

This paper presented the design, analysis and simulation of a received signal strength indication based localization algorithm that uses a path loss model to translate the power measurements to logarithmic ranges that are in turn used directly in the filtering process. The work builds on the approach proposed in [7], while introducing the novelty of the direct inclusion of the signal strength measurements without conversion to distances.

The performance and consistency of the algorithm were validated in a simulated environment with realistic noise showing the convergence of the uncertainty in every variable, as well as the consistency of the said uncertainty with the estimation error.

Future work may include the addition of extra sensors, such as odometry, to improve the estimation due to the variability of the wireless measurements with antenna orientation and other environmental factors. Furthermore, obtaining experimental results of the proposed algorithm in action is important for scientific validation.

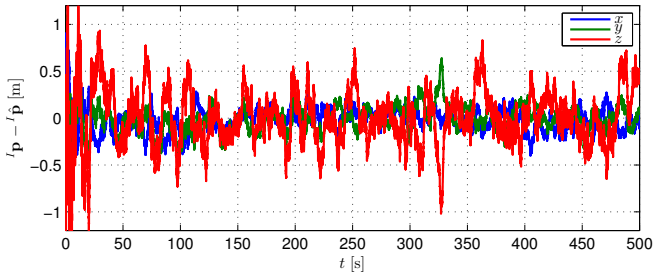

(a) Position.

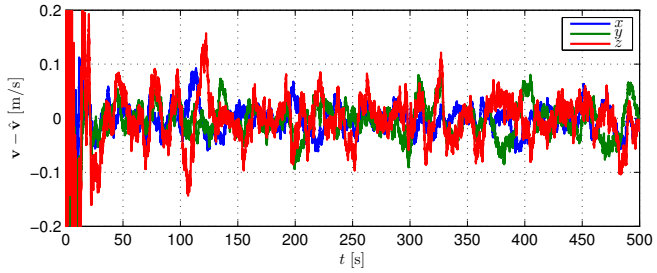

(b) Velocity.

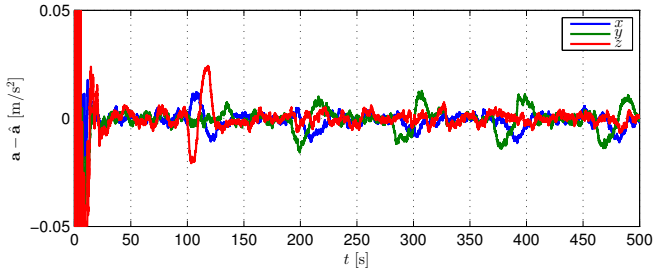

(c) Acceleration.

Fig. 5. Estimation errors for the main state variables.

References

[1] A. Bose and C. H. Foh, "A practical path loss model for indoor wifi positioning enhancement," in *6th International Conference on Information, Communication and Signal Processing*, Singapore, December 2007.

[2] A. Howard, S. Siddiqi, and G. S. Sukhatme, "An experimental study of localization using wireless ethernet," in *4th International Conference on Field and Service Robotics*, Japan, July 2003.

[3] J. Biswas and M. Veloso, "WiFi localization and navigation for autonomous indoor mobile robots," in *2010 IEEE International Conference on Robotics and Automation (ICRA)*, 2010, pp. 4379–4384.

[4] Y. Chen and H. Kobayashi, "Signal strength based indoor geolocation," in *IEEE International Conference on Communications*, vol. 1, New York, USA, May 2002, pp. 436 –439.

[5] V. Matellán, J. M. C. nas, and O. Serrano, "WiFi localization methods for autonomous robots," *Robotica*, vol. 24, pp. 455–461, 6 2006.

[6] A. R. Sandeep, Y. Shreyas, S. Seth, R. Agarwal, and G. Sadashivappa, "Wireless network visualization and indoor empirical propagation model for a campus wi-fi network," *World Academy of Science, Engineering and Technology*, vol. 42, pp. 730–734, 2008.

[7] P. Batista, C. Silvestre, and P. Oliveira, "A Sensor-based Long Baseline Position and Velocity Navigation Filter for Underwater Vehicles," in *Proc. of the 8th IFAC Symposium on Nonlinear Control Systems*, University of Bologna, Italy, September 2010, pp. 302–307.

[8] M. Hata, "Empirical formula for propagation loss in land mobile radio services," *IEEE Transactions on Vehicular Technology*, vol. VT-29, no. 3, pp. 317–325, 1980.

[9] P. Batista, C. Silvestre, and P. Oliveira, "Single range aided navigation and source localization: Observability and filter design," *Systems & Control Letters*, vol. 60, no. 8, pp. 665 – 673, 2011.

[10] P. Batista, C. Silvestre, and P. Oliveira, "A Sensor-based Long Baseline Position and Velocity Navigation Filter for Underwater Vehicles," *ArXiv e-prints*, May 2010.

[11] R. Brockett, *Finite Dimensional Linear Systems*, ser. Series in decision and control. John Wiley & Sons, 1970.